Multi-Objective Synthesis of Antennas from Special and Conventional Materials

Zbyněk RAIDA, Petr KADLEC, Peter KOVÁCS, Jaroslav LÁČÍK, Zbyněk LUKEŠ, Michal POKORNÝ, Petr VŠETULA, David WOLANSKÝ

Dept. of Radio Electronics, Brno University of Technology, Purkynova 118, 612 00 Brno, Czechia

raida@feec.vutbr.cz

Abstract. *In the paper, we try to provide a comprehensive look on a multi-objective design of radiating, guiding and reflecting structures fabricated both from special materials (semiconductors, high-impedance surfaces) and conventional ones (microwave substrates, fully metallic antennas). Discussions are devoted to the proper selection of the numerical solver used for evaluating partial objectives, to the selection of the domain of analysis, to the proper formulation of the multi-objective function and to the way of computing the Pareto front of optimal solutions (here, we exploit swarm-intelligence algorithms, evolutionary methods and self-organizing migrating algorithms).*

The above-described approaches are applied to the design of selected types of microwave antennas, transmission lines and reflectors. Considering obtained results, the paper is concluded by generalizing remarks.

Keywords

Semiconductor antennas, conical antennas, planar antennas, fractal antennas, multi-objective optimization, evolutionary algorithms, swarm intelligence algorithms, self-organizing migrating algorithms, antenna measurements.

1. Introduction

The design of today's antennas is a complex task comprising radiation properties, polarization properties, impedance matching, size constraints, economical aspects and other criteria. From that reason, a multi-objective approach to the antenna optimization is more and more demanding [1.1] – [1.6].

Multi-objective optimization is usually associated with a proper global optimizer. Most today's global optimizers exploit evolutionary principles: a swarm (a generation) of copies of the optimized structure is modified such a way so that the quality of these copies is improved (i.e., the copies are approaching the optima).

Evolutionary algorithms [1.7] and swarm intelligence algorithms [1.8] belong to most popular global optimizers.

Basic principles of evolutionary algorithms and swarm intelligence algorithms are similar:

1. The optimized structure (an antenna, e.g.), which is described by properly chosen state variables (dimensions, electric properties of materials used, magnetic properties of materials used, etc.), is cloned to several identical copies differing in values of state variables.

2. Each copy of the optimized structure is analyzed, and partial criteria of the optimization are evaluated.

3. State variables of copies of the optimized structure are modified to reach the optima as efficiently as possible. In this process, copies with good evaluation play a stronger role than copies with poor evaluation.

4. The optimization returns to 2 to newly evaluate modified copies of the optimized structure.

The partial criteria of the optimization can be conflicting: e.g., a requirement of a high gain is in a conflict with a demand of as smallest size of the antenna as possible. Then, the optimization results form a set of optimal solutions (so called Pareto front of optimal solutions). Some solutions fit the first criterion closer (antennas exhibit a higher gain but their dimensions are larger), other solutions meet the second criterion better (antennas excel in small dimensions but their gain is poorer).

Good multi-objective optimization approaches can accurately identify the Pareto front and cover it by equidistant solutions [1.9].

In order to perform a multi-objective design of an antenna, a proper full-wave solver evaluating partial criteria of the optimization has to be exploited. Depending on the nature of the design, the following selections have to be done:

- **Integral solver versus differential one.** Integral solvers are usually used for the analysis of open structures because the integral formulation comprises all the space surrounding the analyzed structure. Unfortunately, integral solvers are not able to handle with the structures of complicated geometries comprising different dielectrics of an arbitrary shape [1.10], [1.11]. On the other hand, differential solvers can be

used for the analysis of electromagnetic structures of general geometry but special techniques have to be applied for converting an open structure to a closed one [1.12], [1.13].

- **Time domain versus frequency domain**. Frequency domain solvers repeat the analysis of the electromagnetic structure of interest at each harmonic frequency separately; such an approach works well in case of narrow-band structures. On the other hand, time-domain solvers assume a pulse excitation of the analyzed structure; a short pulse can excite a wide spectrum of frequencies, and the response on all the frequencies is obtained in a single run of the time-domain method.

The numerical, multi-objective design of electromagnetic structures is illustrated by several examples in the following chapters. Each chapter is started by the description of the designed structure and its properties. Considering the properties of the designed structure, a proper solver is selected to obtain accurate results in reasonable time.

Next, the optimization criteria are carefully formulated and discussed. Considering the partial objectives, a multi-objective function to be optimized is composed.

Finally, an iterative process of the global optimization is run, and obtained results are documented. Attention is turned to convergence properties of the optimization and to the comparison of required properties and obtained ones.

Chapter 2 is devoted to the optimization of a slot antenna array in the time domain. Slot radiation is described analytically, and the structure is optimized by a novel multi-objective self-organizing migrating algorithm.

In Chapter 3, optimization of a bow-tie antenna in the time domain is described. The antenna is analyzed by the time domain method of moments. Objective functions are composed directly in the time domain and minimized by particle swarm optimization.

Chapter 4 deals with the design of electromagnetic band gap structures and artificial magnetic conductors, generally called *high impedance surfaces*. The dispersion diagram and the reflection phase of the periodic structure are evaluated by analyzing a single element of the planar structure by finite integration technique and finite elements. The analyzed element is surrounded by periodic boundary conditions to truncate the infinite surface into finite dimensions. Multi-objective problem is handled by particle swarm optimization method.

In Chapter 5, a fractal multiband antenna is analyzed by the transient finite integration technique, time domain results are converted to the frequency domain where the multi-objective problem is formulated. Optimal solutions are computed by the scaled probabilistic crowding real-coding genetic algorithm with pattern-centric normal recombination operator.

In Chapters 6 and 7, a similar approach is used for the design of wideband conical antennas and planar arrays.

In Chapter 8, a multi-physical numerical model of a semiconductor structure, suitable to construct active radiators and waveguiding structures is developed to combine electromagnetic fields, particle physics and thermal fields. In order to start the optimization, a parametric analysis has been performed, and the conclusions from this analysis were presented.

Chapter 9 concludes the paper by summarizing generalized remarks on the numerical multi-objective design of radiating (and reflecting) structures.

The research described in this paper was a part of the COST Action IC0603 Antenna systems and sensors for information society technologies (ASSIST). A comprehensive look on the numerical multi-objective design of antenna structures belonged to the important aims of the Action. The study published in this paper is going to contribute to this aim.

2. Adaptive Beam Forming

Shape of the beam radiated by an antenna can be adaptively changed directly in time domain [2.1]. This phenomenon can be observed when excitation pulses of individual elements of an antenna array are delayed. The radiated energy can be focused to a desired domain of space and can vanish in other parts of the space at the same time. This approach meets requirements of a biomedicine hyperthermia [2.2]. In the paper [2.3], parameters of the antenna array feeding are optimized using a novel stochastic optimization algorithm called MOSOMA (Multi-Objective Self-Organizing Migrating Algorithm).

The 2D model of a slot antenna array used for the optimization is depicted in Fig. 2.1. Here, D specifies the computational domain, which is irradiated by the antenna array. The computational domain is filled with a vacuum. A perfectly conducting screen contains five non-overlapping slots A_n. The n-th slot is defined: $\{a_n < x_1 < b_n, x_3 = 0\}$ with respect to $a_1 < b_1 < a_2 < \ldots < b_n$. All slot antennas have the same width w and are in fixed positions with spacing $w/2$. All slots are excited with a power exponential pulse V that can be described by

$$V(t) = V_{max}\left(\frac{t}{t_r}\right)^{v} \exp\left[-v\left(\frac{t}{t_r}-1\right)\right] H(t-T) \quad (2.1)$$

where V_{max} denotes the pulse amplitude, t denotes time, t_r means the rise time when the pulse reaches its amplitude V_{max}, $v > 0$ is so called rising exponent, H (.) assigns the Heaviside step function and T is the start time of the pulse.

The field components $\{E_1, E_3, H_2\}$ can be evaluated using the closed-form expressions derived in [2.4] with use of the Cagniard-DeHoop technique:

$$\{E_1, E_3, H_2\} = \sum_{n=1}^{N} \frac{V_n}{b_n - a_n} *$$

$$\left[\frac{1}{\pi} \left\{ \frac{x_3(x_1 - b_n)}{c^2 t^2 - x_3^2}, 1, \frac{1}{\mu_0} \frac{(x_1 - b_n)t}{c^2 t^2 - x_3^2} \right\} \frac{H(t - T_{b,n})}{\sqrt{t^2 - T_{b,n}^2}} \right.$$

$$- \frac{1}{\pi} \left\{ \frac{x_3(x_1 - a_n)}{c^2 t^2 - x_3^2}, 1, \frac{1}{\mu_0} \frac{(x_1 - a_n)t}{c^2 t^2 - x_3^2} \right\} \frac{H(t - T_{a,n})}{\sqrt{t^2 - T_{a,n}^2}} \qquad (2.2)$$

$$\left. + \left\{ 1, 0, \sqrt{\frac{\varepsilon_0}{\mu_0}} \right\} \left[H(x_1 - b_n) - H(x_1 - a_n) \right] \delta\left(t - \frac{x_3}{c} \right) \right]$$

where * denotes the time convolution, c denotes velocity of light in vacuum, $T_{a,n}$ is the time of arrival from the edge denoted a_n of the n-th slot and δ (.) is the Dirac pulse. Every component contains the convolution integral that can be solved numerically. Two components of the Poynting vector can be computed:

$$S_1 = -E_3 H_2, \quad S_3 = E_1 H_2. \qquad (2.3)$$

In order to model the requirements of the hyperthermia, the optimization is aimed to focus the radiated energy into the point P_{max} $\{x_1 / w = 2.25, x_2 / w = 6.25\}$ and minimize the radiated energy in P_{min} $\{x_1 / w = 0, x_2 / w = 6.25\}$ for time $t / t_n = 10$, where $t_n = w / c$. Following these goals, two objective functions should be minimized:

$$f_1 = -\sqrt{\left(S_1(P_{max})/S_n\right)^2 + \left(S_3(P_{max})/S_n\right)^2} \qquad (2.4)$$

$$f_2 = \sqrt{\left(S_1(P_{min})/S_n\right)^2 + \left(S_3(P_{min})/S_n\right)^2} \qquad (2.5)$$

where S_n is the maximum value of Poynting vector of the TEM mode in a parallel plate waveguide used for the feeding of the apertures.
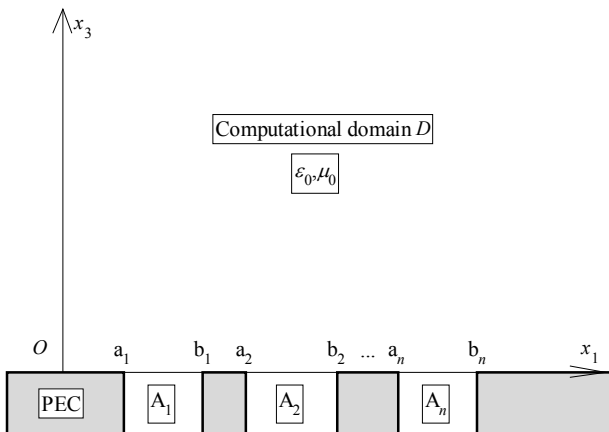
Fig. 2.1. Configuration of the antenna array [2.3].

Objective functions (2.4) and (2.5) are optimized using the MOSOMA. Detailed information about this stochastic algorithm can be found in [2.5]. This algorithm works with group of individuals. All members of the group are non-dominantly sorted to found the possible members of Pareto front. Every agent than migrates towards mem-

bers of the so called external archive that contains all candidates to be Pareto front members. This migration proceeds in the multi-dimensional space of optimized parameters. Agents share the information about values of fitness functions in visited places.
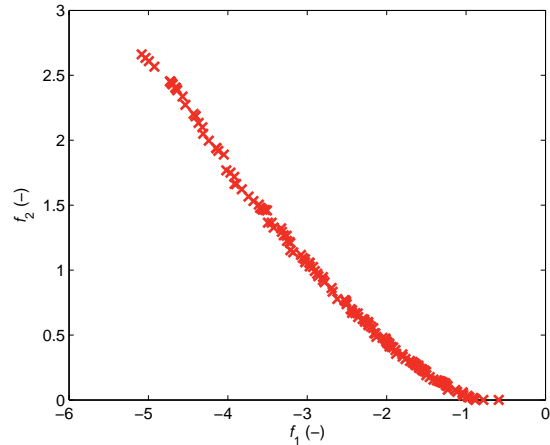
Fig. 2.2. Pareto front of the optimized problem found by the MOSOMA.

Within the optimization process, 14 parameters are changed: excitation times of four slot antennas, amplitudes and rise times of all five excitation pulses $\{T_2, \ldots, T_5, V_{max,1}, \ldots, V_{max,5}, t_{r,1} \ldots, t_{r,5}\}$. All times are expressed as multiples of t_n. The resulting Pareto front from Fig. 2.2 expresses the trade-off between both objectives.
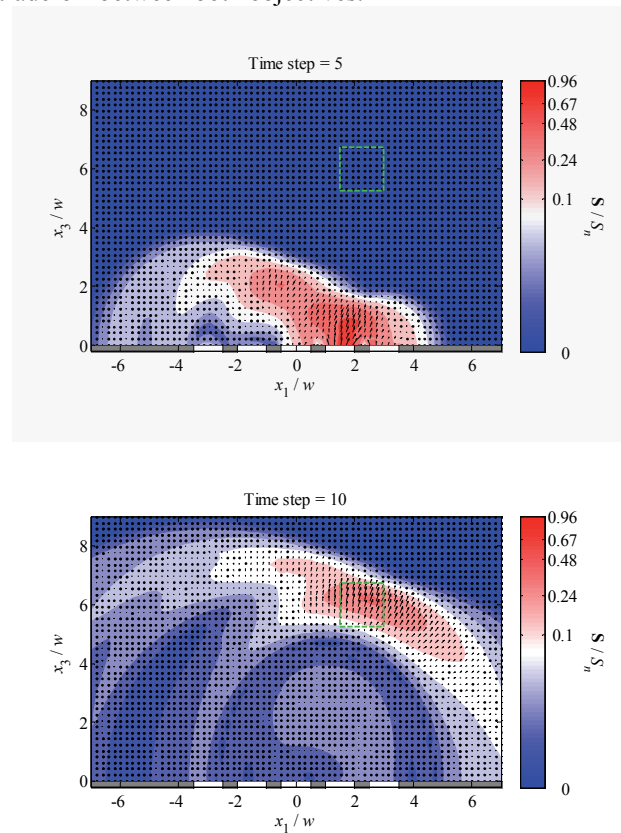
Fig. 2.3. Time evolution of the radiated field for optimized feeding of the focused antenna array.

The radiated field in the computational domain for two times of the solution lying in the middle of the Pareto front {0.5, 1.0, 2.0, 2.0, 1.0, 1.0, 1.0, 1.0, 1.0, 1.5, 1.44, 1.5, 1.5, 1.35} is shown in Fig. 2.3.

If the excitation pulses resulting from the optimization are repeated with an appropriate period, the tissue is heated in some regions while other parts of the tissue stay unheated. Thanks to the formulation of the objective functions, the field components need to be computed only in two points at one time which speeds up the process. Also the use of exact closed-form expressions decreases the time devoted to the whole optimization.

Conclusion. In order to model a slot array operating in pulse regime, time-domain integral approach is used. Integrating time domain responses, power in observation points is computed. Conflicting objectives requesting minimum power and maximum power in specified points are met by applying the MOSOMA algorithm. The described global multi-objective time-domain beam forming is an original contribution.

3. Time Domain Optimization of Bow-Tie Antenna

The bow-tie antenna belongs to the class of broadband antennas. The bow-tie antenna is made from metal, and is defined by its length L, the width of the feeding strip w, and the arm angle α (Fig. 3.1). These parameters are used as the state variables in the optimization task.

Since antennas are open structures and the bow-tie antenna is simple, the analysis is performed in the time domain by applying TD-EFIE [3.1]. Here, the marching-on-in-order scheme is utilized [3.2].
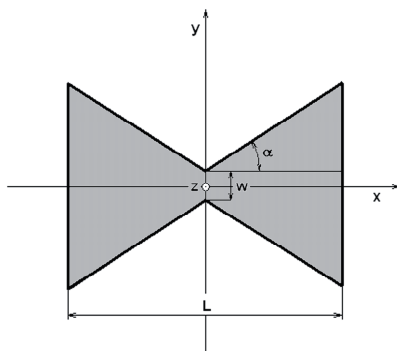
Fig. 3.1. Bow-tie antenna and definition of its parameters.

Unfortunately, conventional antenna parameters are defined in the frequency domain. In order to avoid the Fourier transformation of the time response at each step of an optimization procedure, we exploit the objective function defined in the time-domain directly [3.3].

For a given excitation pulse, the time-domain objective function [3.3] can take into account the "time-domain

impedance matching", a distortion of responses at the feeding point and in a desired radiating direction (with respect to the excitation pulse), and the radiated energy in the desired direction

$$OF = \left\{ \left(1 - FF_0 \right)^2 + \left(1 - MY \right)^2 + \\ + \left[1 - FE_{max} \left(\vartheta_d, \varphi_d \right) \right]^2 + \\ + \left[1 - E_{Enorm} \left(\vartheta_d, \varphi_d \right) \right]^2 \right\}^{\frac{1}{2}} \quad (3.1)$$

where FF_0 is the fidelity factor of the excitation pulse and the response at the feeding point of the antenna, MY is the time domain matching factor, FE_{max} is the fidelity factor of the excitation pulse and the radiated pulse in the desired direction defined by the angles ϑ_d and φ_d, E_{Enorm} is normalized radiated energy in the desired direction.

Values of all these parameters belong to the interval from 0 to 1. All requirements are met if the objective function (3.1) is zero. That is the absolute minimum of this function.

We will exploit the objective function (3.1) and design the bow-tie antenna that is matched to a feeding line with the admittance $Y_W = 10$ mS in the frequency range from 2 to 4 GHz. The antenna is required to radiate energy uniformly within the given frequency range in the direction $\varphi_d = 0°$, and $\vartheta_d = 0$ (perpendicularly to the plane of the drawing in Fig. 3.1), and to ensure maximum radiation in that direction.

For optimization, the harmonic signal at the frequency 3 GHz modulated by the Gaussian pulse of the width 2.4 ns is used. Such a pulse covers an important part of the spectrum from 2 to 4 GHz.

State variables can vary in intervals: $L \in$ <100 mm; 190 mm>; $w \in$ <5 mm; 15 mm>; $\alpha \in$ <30°; 70°>.

The particle swarm optimization (PSO) [3.4], which exploits the numerical model for evaluating the objective function, is used in its conventional form. A swarm consists of 15 agents, and the optimization runs for 70 iterations. The inertial weight is linearly decreasing from the value 0.9 in the initial iteration to the value 0.4 in the last one. Both the personal scaling factor and the global one are set to 1.49. The absorbing walls are used.

The evolution of the objective function is depicted in Fig. 3.2. For the final iteration, the objective function reaches the value $OF = 0.0535$, with the partial criterions amounting to $|1 - FF_0| = 0.04498$, $|1 - MY| = 0.0094$, $|1 - FE_{max}(\varphi_d, \vartheta_d)| = 0.0274$ and $|1 - E_{Enorm}(\varphi_d, \vartheta_d)| = 0$. Correspondingly, the entries in the optimized state variables vector are: $L = 112.48$ mm, $w = 13.17$ mm and $\alpha = 64.27°$.

The transient responses of the current at the feeding point of the antenna and the radiated pulse in the desired direction, both normalized to the square root of their autocorrelation functions at $t = 0$ s, are shown in Fig. 3.3 and

3.4, respectively. For comparison, the excitation pulse is normalized in the same way as the responses.
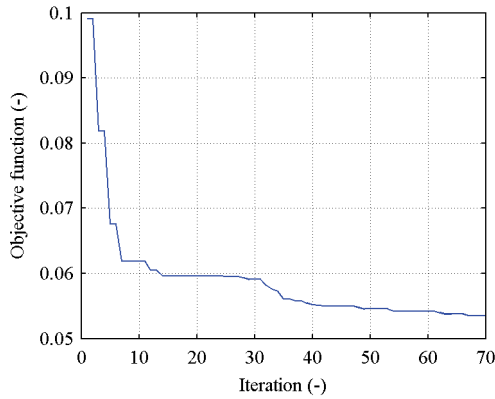
Fig. 3.2.   Evolution of objective function.
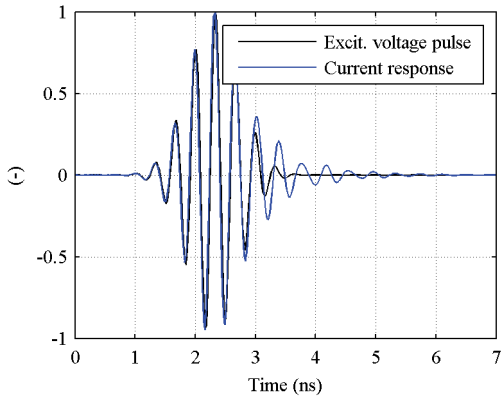
Fig.3.3.   Normalized excitation voltage pulse and current response of the optimized antenna.
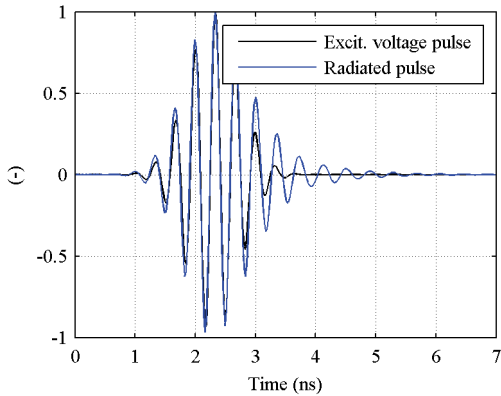
Fig. 3.4.   Normalized excitation and radiated pulses of the optimized antenna.

The computed return loss parameter S_{11} for the excitation pulse and the current response is depicted in Fig. 3.5 (denoted by TD) after mapping the results to the frequency domain. Apparently, the optimized antenna is very well matched to the feeding line.

For the verification of the antenna radiation in the desired direction, the magnitude of the transfer function (the ratio of the spectrum of the radiated pulse and the excitation pulse is computed) normalized to its maximum is

depicted in Fig. 3.6. Obviously, the minimum radiation corresponds to the frequency 4 GHz.
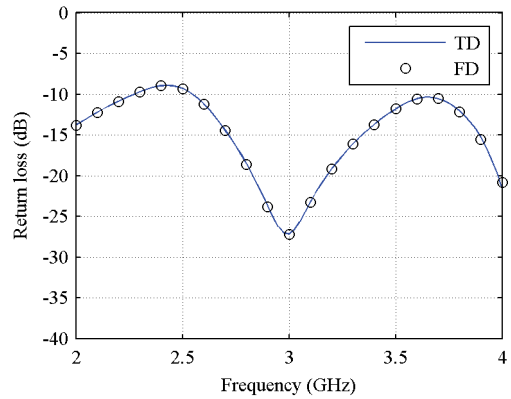
Fig. 3.5.   Return loss of optimized bow-tie antenna.
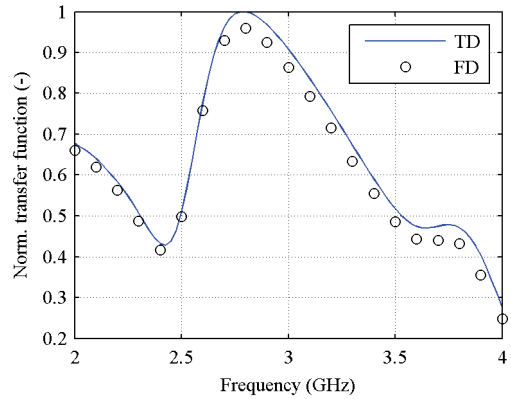
Fig. 3.6.   Normalized transfer function of optimized bow-tie antenna.

For the verification, the optimized bow-tie antenna was analyzed by the method of moments in the frequency domain [3.5] (denoted in Fig. 3.5 and 3.6 by FD). The agreement of both solutions is good.

Obviously, the optimized antenna exhibits favorable characteristics.

Conclusion. In order to model a wideband antenna, time-domain integral solver is used. Design requirements are expressed by three time-domain objectives, which are associated into a single objective function (requirements of impedance matching, pulse distortion and pattern properties are not conflicting). The optimum is computed by particle swarm optimization. The described concept of the multi-objective optimization, which is fully performed in the time domain, is an original contribution. Frequency domain transform is applied to the results only to check the optimization outputs.

4.   Design and Optimization of High-Impedance Surfaces

An intensive interest in periodic structures in antenna engineering has been recently observed. A kind of metallo-

dielectric periodic structure called high-impedance surfaces (HIS) enables one to design low-profile antennas and substrates with suppressed surface wave propagation due to their artificial magnetic conductor (AMC) and electro-magnetic band gap (EBG) properties, respectively [4.1].

For many applications, simultaneous AMC and EBG behavior of HIS is required. However, the design of such a structure is quite difficult because of the large factor of uncertainty on how the properties of the structure change their dependence on unit cell geometry. Moreover, both the frequency of the zero reflection phase, and the position of the surface wave band gap can alter separately [4.2].

Let us turn the attention to the design of a conventional mushroom HIS [4.1] for simultaneous AMC and EBG operation at frequency 10.25 GHz. The unit cell for the optimization including the state variables (period D, the size of the square metallic patch P and the diameter of the via d) is depicted in Fig. 4.1. The structure is realized on the dielectric substrate Arlon AD600 with a relative permittivity $\varepsilon = 6.15$ and thickness $h = 1.575$ mm.
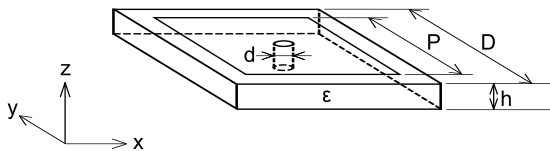
Fig. 4.1. The mushroom unit cell.

The mushroom unit cell was optimized using the particle swarm optimization (PSO) implemented in Matlab in connection with the finite-integral technique (FIT) of CST Microwave Studio (CST MWS) for the dispersion diagram calculation (eigenfrequency analysis) and the reflection phase computation (time domain analysis). The PSO was chosen because of the fastest convergence in comparison with other optimization methods [4.3]. The objective function F is composed of two partial objective functions F_1 and F_2 and is going to be minimized

$$F = F_1^2 + F_2^2 . \qquad (4.1)$$

The first partial objective function F_1 is formulated as a two-criterion function with respect to both the band gap position and the maximum bandwidth

$$F_1 = w_1 \cdot \left(\frac{f_{BG1} + f_{BG2}}{2} - f_C \right)^2 -$$
$$- w_2 \cdot \left(\frac{f_{BG2} - f_{BG1}}{2} \right) + q . \qquad (4.2)$$

The second partial objective function F_2 considers the frequency of the zero reflection phase

$$F_2 = w_3 \cdot \mathrm{abs}\left(f_{AMC} - f_C \right). \qquad (4.3)$$

In equations (4.2) and (4.3) w_1, w_2 and w_3 denote weighting coefficients ($w_1 = 1$ GHz^{-2}, $w_2 = 0.25$ GHz^{-1}, $w_3 = 1$ GHz^{-1});

f_C is the required central frequency of the band gap ($f_C = 10.25$ GHz); f_{BG1} and f_{BG2} (in GHz) are the lower and the upper limit of the band gap, respectively; q is a constant ($q = 1$); and f_{AMC} (in GHz) is the frequency of the zero reflection phase.

	f_{BG1}	f_{BG2}	f_{AMC}
CST MWS	9.0 GHz	11.1 GHz	10.3 GHz
Ansoft HFSS	9.1 GHz	11.1 GHz	10.3 GHz
Measurement	9.5 GHz	11.5 GHz	10.7 GHz

Tab. 4.1. Optimization and measurements results.

An evaluation of the objective function F and the band gap position and frequency of the zero reflection phase were monitored during the optimization process (Fig. 4.2). The optimum ($D = 2.22$ mm, $P = 2.04$ mm and $d = 0.40$ mm) was firstly checked by the finite-element solver Ansoft HFSS, and then successfully confirmed by measurements (Fig. 4.3 and Fig. 4.4). The obtained results are summarized in Tab. 4.1. Obviously, the described methodology could be a very helpful tool in the design of more complex periodic structures.
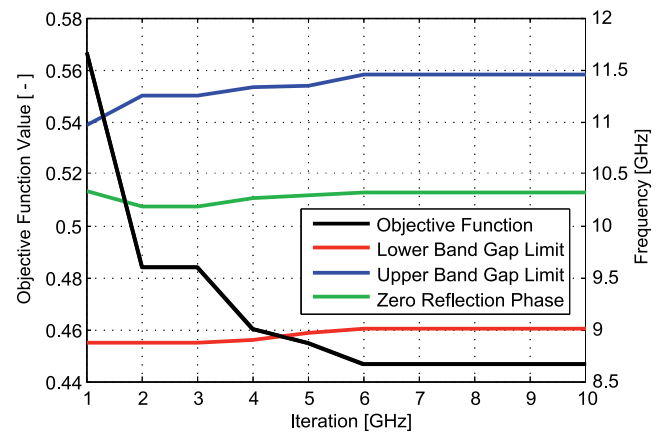
Fig. 4.2. Optimizing the mushroom unit cell: evaluation of objective function, position of band gap and frequency of zero reflection phase.
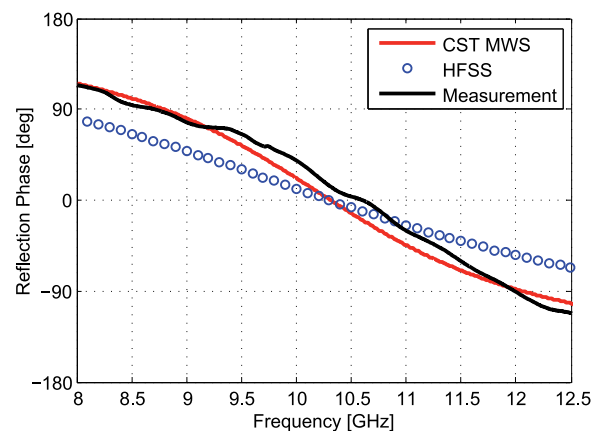
Fig. 4.3. Calculated and measured reflection phase curves of the designed HIS.
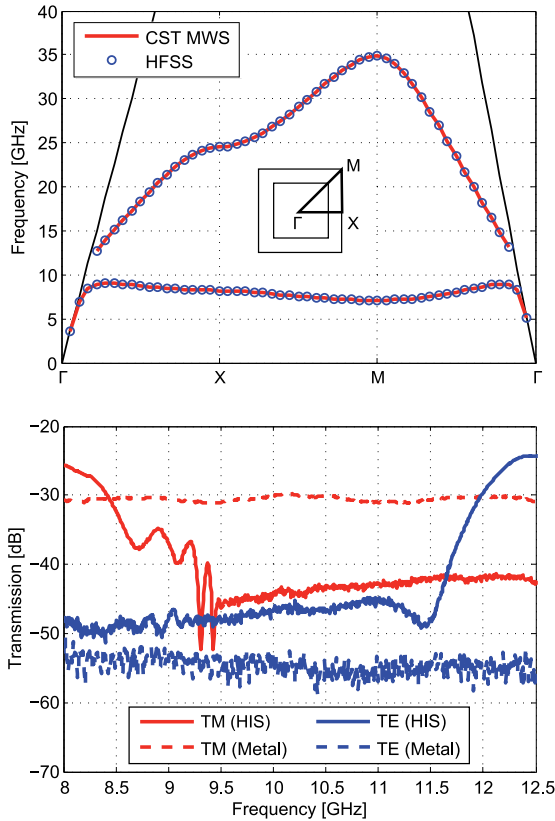
Fig. 4.4. Dispersion diagram of the designed HIS (top); measured TM and TE surface waves transmission curves over the designed HIS versus the conventional metal ground plane (bottom).

<u>Conclusion</u>. The analysis of HIS was performed in two different domains: the dispersion diagram was evaluated in the eigenfrequency domain and the reflection phase in the time domain. Since there is no conflict between the dispersion properties and phase properties, objectives are combined into a common cost function. An optimum is computed by PSO. A multi-domain objective function is a unique feature for the developed synthesis methodology.

5. Synthesis of Multi-band Koch Discone Antenna

The Koch fractal is created by several scaled-down and rotated copies of a basic motive. The Koch dipole and the Koch snowflake are the basic representatives of Koch antennas [5.1]. The reduced size and the multi-band behavior are the important advantages of Koch antennas.

In this section, the Koch fractal is applied to a shape of a discone antenna to widen the bandwidth of the antenna. The resultant discone antenna is analyzed in CST Microwave Studio (time domain finite integration technique) to perform the wideband analysis efficiently. After the analysis, the transient data are mapped into the frequency domain by Fourier transform. That way, the desired frequency-domain parameters of the analyzed antenna are obtained.

The antenna is optimized by the scaled probabilistic crowding real-coding genetic algorithm with pattern-centric normal recombination operator (SPC-PNX) [5.2], [5.3]. SPX-PNX performs better on functions having several minima, and poorer on unimodal functions. In a fact, the optimization of the designed antenna is more efficient using SPX-PNX than other real and binary coded optimization techniques.

The wideband objective function can be evaluated according to

$$c(\mathbf{x}) = w_1 c_1(\mathbf{x}) + w_2 c_2(\mathbf{x}) + w_3 c_3(\mathbf{x}) \qquad (5.1)$$

where $c(\mathbf{x})$ is the global objective function of the state vector $\mathbf{x}$, c_1 is the objective function for wideband impedance matching of the antenna, c_2 is the low band impedance matching (we emphasize the optimization of the antenna at lower frequencies rather than at higher ones), c_3 is the objective function describing the gain of the antenna and w_1, w_2 and w_3 are weighting coefficients.

The local objective function c_1 is given by

$$c_1 = \frac{1}{N} \sum_{i=fmin}^{fmax} \sqrt{\left[Z_{re}(i) - Z_{0re}\right]^2 + \left[Z_{im}(i) - Z_{0im}\right]^2} \qquad (5.2)$$

where N is the number of frequencies considered in the design (in our case, we exploited the set of 1001 frequency samples), f_{min} is the lower bound of the frequency interval of the optimization, f_{max} is the upper bound of the frequency interval of the optimization, Z_{re} is the real part of the computed input impedance, Z_{im} is the imaginary part of the computed input impedance, $Z_{0re} = 50\ \Omega$ and $Z_{0im} = 0\ \Omega$ are required values of the input impedance of the antenna.

The second objective function is identical with (5.2), but f_{max} is limited to one tenth of the bandwidth. This objective function ensures that the antenna is matched at lower frequencies better.

The third objective function c_3 is evaluated according to

$$c_3 = \left[\sum_{i=fmin}^{fmax} G_i \right]^{-1} \qquad (5.3)$$

where G_i [dB] is the gain in the horizontal plane in the main lobe direction.

The vertical cut of the antenna is depicted in Fig. 5.1. During the optimization, the number of fractal iterations, the length of the antenna L and the radius of the antenna a are changed. The *SPC-PNX* [5.2], [5.3] was run with the number of offspring $\Lambda = 1$ and the PNX parameter $\eta = 2$. The population consisted of 10 individuals and the maximum number of iterations was set to 50.

The antenna was optimized in the frequency range from 1 GHz to 6 GHz. When the criteria function dropped below 50 (the average value of PSV < 1.5, and the gain > 2 dBi) the optimization was finished. The model con-

sisted of about 500 thousands cells, and one simulation run took 3 minutes approximately.
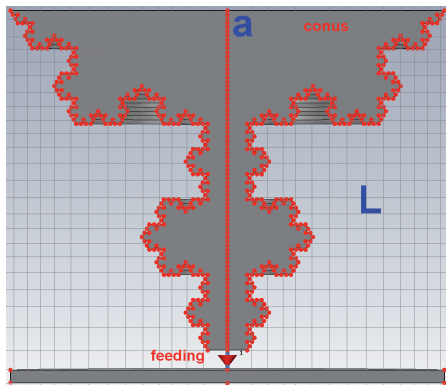
Fig. 5. 1. Vertical cut of the Koch discone antenna for $N = 4$.

In Fig. 5.2, evolution of the global cost function is depicted. The optimum number of fractal iterations is 5, the optimum length of the antenna $L = 23.6$ mm and the optimum radius of the antenna $a = 47.4$ mm.
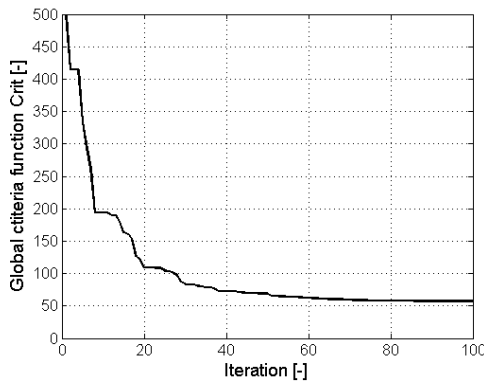
Fig. 5.2. The best evolution of cost function of the Koch discone antenna optimized by SPC-PNX.

Fig. 5.3 shows frequency response of the return loss of the optimized antenna. The return loss is lower than −12 dB in almost the whole frequency range of operation.
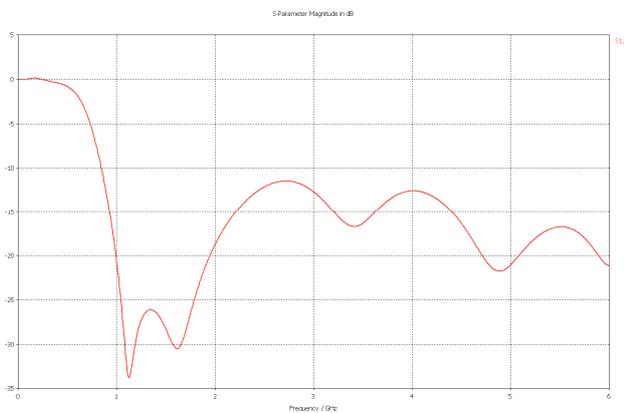
Fig. 5.3. Frequency response of return loss at the input of the optimal Koch discone antenna.

In Table 5.1, values of the maximal gain of antenna are listed.

f [GHz]	G [dBi]
1	1.70
2	1.75
3	3.50
4	3.00
5	3.70
6	1.80

Tab. 5.1. Maximum gain in horizontal plane.

Conclusion. The wideband analysis of the Koch discone antenna was performed in the time domain. Results were converted into the frequency domain and used in objective functions. Non-conflicting objectives were associated into a single cost function, which was minimized by SPX-PNX algorithm. The synthesized Koch discone antenna is an original contribution of this section.

6. Wideband Conical Horn Antenna

In this chapter, antennas, which transform the impedance of the coaxial transmission line to the impedance of the open space via the circular waveguide, are described. These antennas are numerically modeled in CST Microwave Studio (transient analysis). The numerical models of the antennas are optimized using optimizers implemented in CST.

The wideband conical antenna is fed by the coaxial transmission line with the characteristic impedance 50 Ω. The outer conductor of the coaxial transmission line is extended to create a conical horn antenna. The antenna is filled by the dielectrics to reduce the dimensions on one hand and to match the input impedance of the antenna on the other hand (see Fig. 6.1) [6.1].
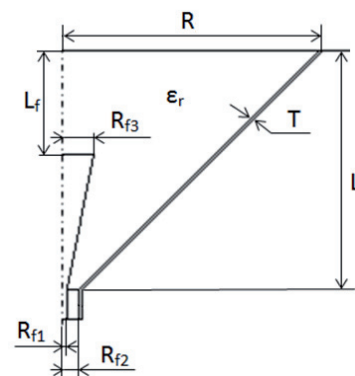
Fig. 6.1. Vertical cut of the conical horn antenna.

Along the coaxial transmission line, the transversally electromagnetic wave is propagating. The φ component of the magnetic field intensity and the r component of electric field are dominant in the aperture [6.2].

In the distance L_f from the aperture, the inner conductor of the coaxial feeder is ended to suppress radial components of the electric field, and therefore, the magnetic field intensity is dominant on the aperture. The φ component of magnetic field intensity simulates a loop of the magnetic current. Considering the duality theorem, the

loop of the magnetic current is equivalent to an electric monopole [6.1], [6.3].

Description	Variable	Unit	Value
Radius of aperture	R	mm	100.00
Radius of inner conductor of coaxial feeder	R_{f1}	mm	0.50
Radius of outer conductor of coaxial feeder	R_{f2}	mm	2.43
Upper radius of inner conductor of coaxial feeder	R_{f3}	mm	0.50
Length of horn	L	mm	100.00
Distance of monopole from aperture	L_f	mm	20.00
Permittivity of dielectric filling of horn	ε_{r1}	-	3.60

Tab. 6.1. Numerical values of variables of the horn antenna.

The numeric values of variables of the antenna are given in Tab 6.1. Frequency response of the return loss of the antenna is depicted in Fig. 6.2.
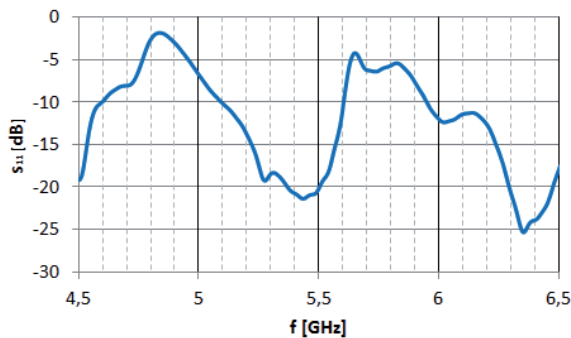
Fig. 6.2. Frequency response of the return loss of the conical horn antenna.

The antenna was optimized to meet impedance matching conditions in the 802.11a band. In that case, a single-objective optimization was performed only. The range of the frequency band of the 802.11a standard is defined from 5.150 GHz to 5.825 GHz.

The first design of the antenna was based on the parametric sweep of dimensions of the antennas. This method was used to found out which parameters dominantly influence the behavior of the antennas.

CST Microwave Studio offers several optimization algorithms. The combination of global and local optimization methods was used to find the optimal solutions. The particle swarm optimization (PSO) was chosen as a global method and Nelder-Mead simplex algorithm (NM) was selected as a local one. The PSO cannot stack at a locally optimal point but is time-consuming. The NM is CPU-time modest but has a tendency to stack in a local optimum.

The optimal values of variables are listed in Tab. 6.2. Frequency responses of the return loss of the optimized antennas are depicted in Fig. 6.3. Here, results are compared with the basic conical horn antenna (see Fig. 6.2).

Variable	Unit	Constant inner conductor	Widened inner conductor
R		37.87	27.53
R_{f3}	mm	0.50	1.63
L		41.33	20.42
L_f		18.44	2.42

Tab. 6.2. Resulting parameters of the optimized conical horn antennas.

The return loss was asked to be $|S_{11}| < -10$ dB in the operation band. In order to meet this goal, the optimization routine computed the upper radius of the antenna R, the length of the whole structure L and the distance of the monopole from the aperture L_f. In the case of the antenna with the widened inner conductor the upper radius of the monopole R_{f3} was also calculated.
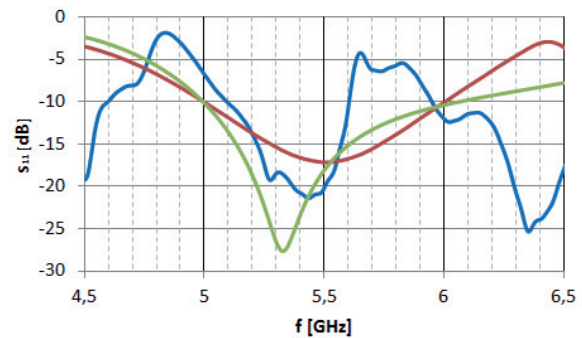
Fig. 6.3. Frequency response of the return loss of the optimized antennas – the basic conical horn antenna (blue), the horn antenna with the constant inner conductor (red) and the horn antenna with the widened inner conductor (green).

The conical horn antennas exhibit the return loss better than –10 dB in the operating band. The antennas excel in the small size and the possibility of placing the ground plane to the plane of the aperture. In the case of the conical horn antenna with the widened inner conductor, almost the half size of the structure was obtained compared with the conical horn antenna with the constant inner conductor. On the other hand, the manufacturing of the conical horn antenna with the widened inner conductor is rather complicated.

Conclusion. The wideband analysis of the antenna of interest was performed in the time domain. Results were converted into the frequency domain. An optimum of a single objective cost function was computed by the global PSO and refined by local Nelder-Mead simplex algorithm. The described concept of the transformation of the coaxial transmission line to an open space via the circular horn antenna is a novel contribution.

7. Antenna Array of E-shaped Patches with Washer

The single E-shaped patch antenna with the washer was published by Ooi [7.1]. The circular washer beneath the lower patch aids to cancel the reactance of the feeding probe and produces better impedance matching of the antenna [7.1].

We remove the upper parasitic patch and the E-shaped patch is placed on dielectric substrate Taconic TLX-8 with thickness 0.51 mm and relative permittivity 2.55. The single element antenna is fed by the microstrip transmission line which is connected to the 50 Ohm SMA connector. The washer is placed on the reverse side of the substrate with the E-shaped patch. The whole antenna is covered by a dielectric radome (ABS) of the relative permittivity 2.77 with thickness 5 mm. Fig. 7.1 shows the schematic model of the single element antenna concept.

The single E-patch antenna was designed and simulated in CST Microwave Studio using finite integration technique in full-wave time-domain solver. The design was aimed to achieve $|S_{11}| \leq -22$ dB for the complete antenna array in the band from 4.4 GHz to 5.0 GHz. That is the reason why the focus is put on impedance matching of the single antenna element. Single E-patch antenna parameters from Fig. 7.1 (top) and H_2, H_3 from Fig. 7.1 (bottom) were optimized to achieve $|S_{11}| \leq -25$ dB in the required band.
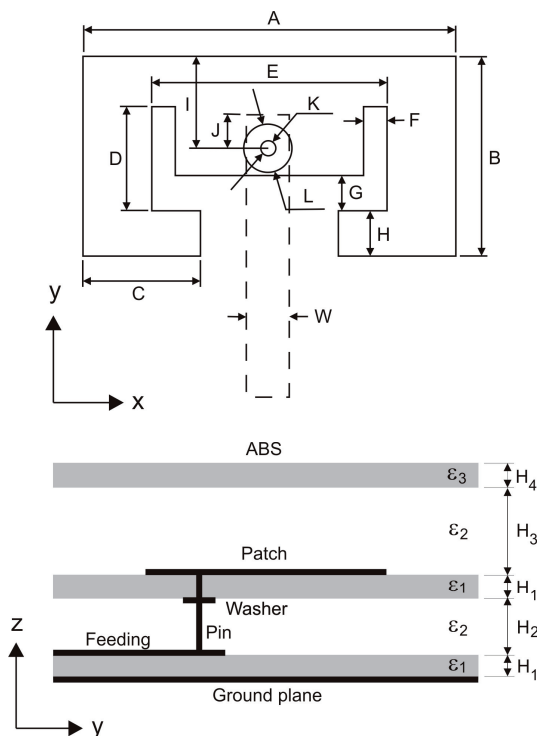
Fig. 7.1. Schematics of the single element of antenna array: top view (top), side view (bottom).

For the need of optimization process, an internal CST optimizer was used. First, the antenna was tuned to the passband by adjusting the length of the slot (the parameter

D in Fig. 7.1) afterwards the antenna was optimized using the local optimization by Nelder-Mead simplex. This method was chosen due to the fast convergence. The disadvantage of this method is the possibility of sticking at the locally optimal point. In this case the global particle swarm optimization (PSO) method was used.

The optimal impedance matching of the antenna element is shown in Fig. 7.2. The realized gain in the passband is $G_1 = 7.6$ dB in average.
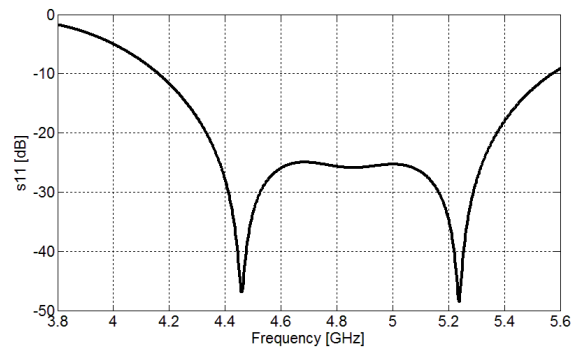
Fig. 7.2. Impedance matching of the single E-shaped patch antenna.
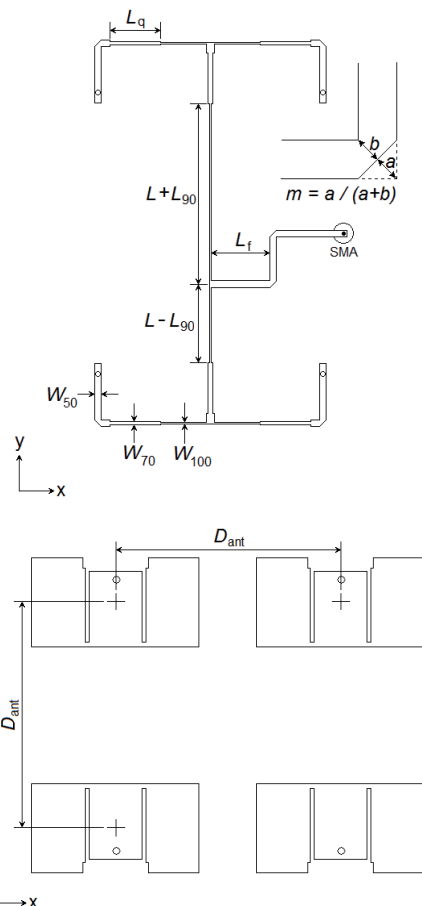
Fig. 7.3. Schematics of the antenna array: feeding network (top), patches (bottom).

In order to achieve higher gain, the single antenna element was arranged into the 2×2 antenna array. The

schematic model of the patches and feeding network is shown in Fig. 7.3. Due to deflection of the main lobe of the single antenna element, the opposite patches are fed with the phase difference of 180°. The antenna is fed by the 50Ohm SMA connector which is connected at the bottom side of the antenna. The distance between the centers of the patches is $D_{ant} \approx 0.7\lambda$ [7.2]

Due to the mutual coupling between adjacent patches, the antenna is relatively untuned and it results in a need to tune the antenna to the required frequency band. Both the dimensions of the feeding network and the dimensions of individual patches are optimized to achieve $|S_{11}| \leq -22$ dB in the required band.

The optimization commenced with the PSO in order to find a solution close to the optimum. Afterwards, the local method Nelder-Mead simplex was used to find the global optimum. During the optimization process the simplex size was decreased in order to find the optimal solution faster.
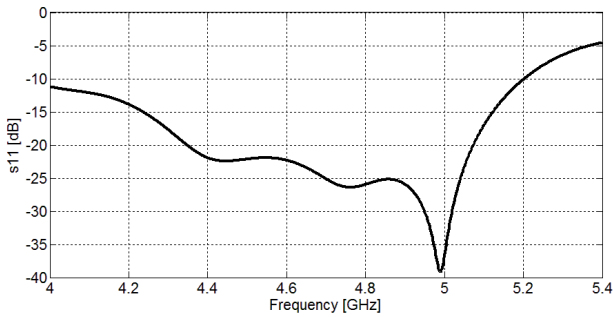
Fig. 7.4. The impedance matching of the antenna array.
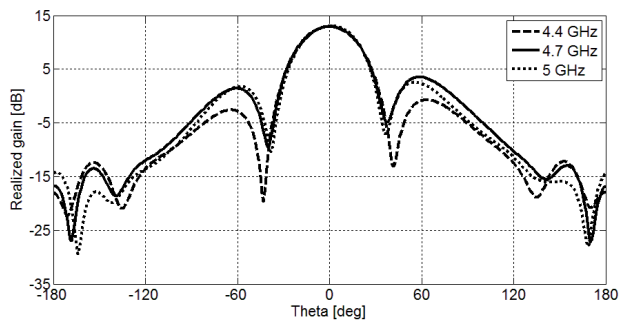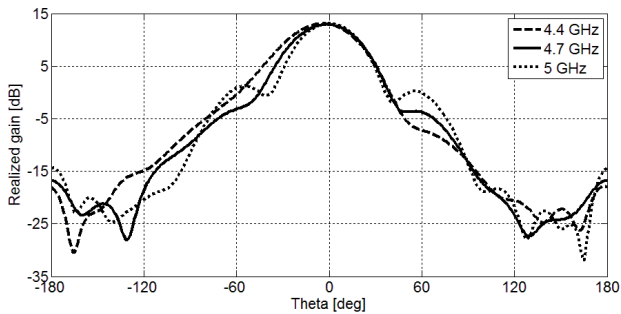
Fig. 7.5. Radiation patterns of the antenna array: E-plane (top), H-plane (bottom).

The optimal impedance matching obtained by the described optimization is depicted in Fig. 7.4. Fig 7.5

shows the radiation patterns of the antenna array in E-plane and H-plane. The realized gain reaches the 13.1 dB for 5.0 GHz.

Conclusion. The wideband analysis of the antenna of interest was performed in the time domain, results were converted into the frequency domain, and an optimum of a single objective cost function was computed by the global PSO and refined by local Nelder-Mead simplex algorithm. The wideband optimization of a complex antenna structure comprising an antenna array, a feeding network and a dielectric radome is a novel contribution of this design.

8. Semiconductor Structure with Distributed Amplification

In this section, a parametric analysis of an active microstrip line based on the traveling wave interaction with the transversal drift of electrons in GaAs semiconductor [8.1], [8.2], [8.3] is performed. This concept has the potential to overcome the principal limitation on output power of the lumped active devices up to frequencies of the intervalley scattering rate limit of GaAs which is estimated to 100 GHz at the room temperature [8.2], [8.4].

We have developed the cross-section model of the 50 Ω active microstrip line on a low n-doped GaAs substrate with thickness of 100 μm (Fig. 8.1), where the highly doped area with the value N_D^+ is shown in red. The structure is biased by voltage V_a at the strip conductor and grounded at heat sink interface.
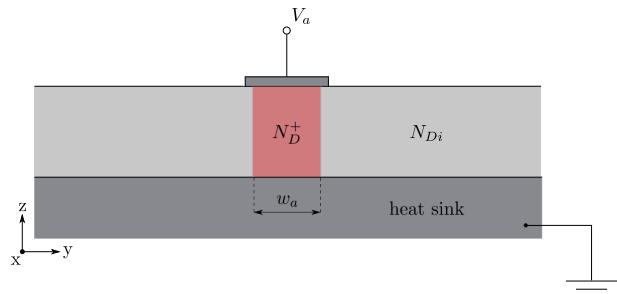
Fig. 8.1. Active microstrip line design on GaAs substrate.

The characterization of such devices cannot be restricted to the EM field analysis. It represents the coupled system of the electromagnetic, particle and thermal fields, which implies a number of objectives on device parameters and requirements to be met to achieve a feasible structure.

Concerning the EM field, the eigenvalue problem formulated by wave equation in frequency domain is solved to obtain the line impedance, attenuation constant and phase constant. The objectives are the minimal attenuation constant α and the maximal working frequency f_T.

The particle field is governed by three equations, the Poisson equation for electrostatic field and two continuity equations of charge carriers transport phenomena. There are no objectives which can be directly formulated using

particle filed quantities. However, there is the requirement of the device stability which can be evaluated as the function of the bias voltage, terminals distance and the electrons distribution along the current density path between terminals [8.3], [8.5].

The thermal field is solved not only in the domain of the semiconductor device, but also in domain of the heat sink and in the domain of surrounding space, where the convection of the air can be assumed. In order of the model complexity reduction, the heat sink can be represented by the heat flux coefficient *htc* at the appropriate boundary [8.3]. The device temperature T affects the physical parameters of the semiconductor substrate and consequently the solution of the particle and EM fields. The objective is to obtain the minimal temperature of device using the feasible value of the *htc* coefficient (value which can be achieved by a real passive heat sink). The requirement is to not exceed the maximal working temperature of GaAs which is 400 K [8.6].

Due to interdisciplinary character of the solved problem we chose the finite element method to analyze the described device in the macroscopic approximation of the electron dynamic [8.3] using COMSOL Multiphysics. The optimization process using common algorithms cannot be used due to extremely time consuming analysis of the structure. Instead, we make a parametric analysis in order to investigate the dependencies of chosen parameters on the defined objectives while the requirements are met. The set of the structure modifications with values of the appropriate parameters are listed in Tab. 8.1.

label	htc [Wm^{2}K^{-1}]	N_D^+ [m^{-3}]	w_a [μm]
I	10^4	1×10^{19}	60
II	10^5	1×10^{19}	60
III	10^4	2×10^{19}	60
IV	10^4	1×10^{19}	30
V	10^5	2×10^{19}	30

Tab. 8.1. Design parameters modification.

The analysis results are presented in Fig. 8.2 and Fig. 8.3. Fig. 8.2 shows the attenuation constant difference $\Delta\alpha$ between active and passive microstrip line at the maximal stable bias voltage V_a. Fig. 8.3 shows the peak temperature characteristics of the device. The values of the objectives are listed in Tab. 8.2. It is clear that the design modification labeled as V represents the device with the best performance.

Conclusion. In this section, a multi-physical model of a semiconductor transmission line is presented. The model comprises electromagnetic fields, thermal fields and particle physics. Due to the complexity of the numerical model, the optimization was replaced by the parametric analysis. Considering results of the parametric analysis, an area containing a potential optimum can be identified, and a proper local optimizer can be applied to compute the local optimum. The described process is under development.

The presented multi-objective model of the semiconductor transmission line with the distributed amplification is original.
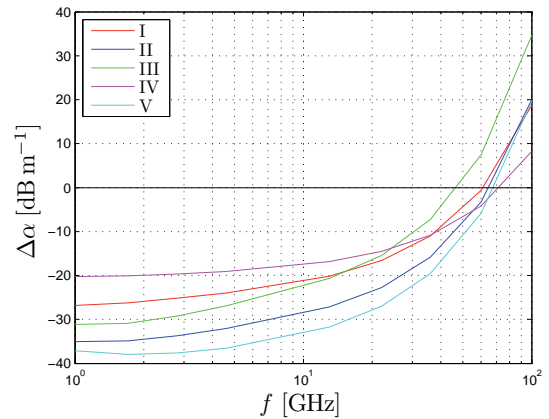
Fig. 8.2. Frequency characteristic of the attenuation constant difference.
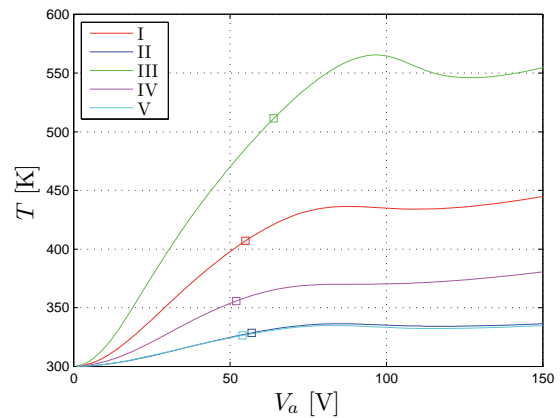
Fig. 8.3. Peak temperature characteristics of devices; rectangles denote the stable device bias V_a.

label	$\Delta\alpha_{max}$ [dBm^{-1}]	f_T [GHz]	V_a [V]	T [K]
I	-26.8	63.3	55	407
II	-35.1	65.6	55	329
III	-31.2	47.8	64	512
IV	-20.2	73.5	52	356
V	-38.0	69.2	54	326

Tab. 8.2. Analysis results of the design modifications.

9. Conclusion

In the paper, several design examples have been presented to tackle different classes of optimization processes of electromagnetic structures (see Tab. 9.1):

• Pulsed structures and wideband structures have been analyzed in the time domain in order to correctly model transient fields (time domain beam forming) or efficiently perform wideband analysis (bow-tie antenna, Koch discone, conical horn, planar antenna system). When needed, several solvers have been

used (time-domain analysis and eigen-frequency analysis in case of high impedance surfaces, and multi-physical analysis in case of semiconductor waveguides).

- Objectives have been formulated in the time domain directly (time domain beam forming, bow-tie antenna) in order to eliminate the necessity of exploiting Fourier transform. In case of complex structures, multi-domain objectives play an important role. Frequency-domain objectives are used in routine designs typically.

- In case of conflicting objectives, the Pareto front of optimal solutions has to be computed (time domain beam forming). In case of non-conflicting objectives, objective functions are connected into a single-objective cost function.

- In order to improve efficiency of global optimization, global optimizers are used to identify subspaces, which can potentially contain a global optimum; identified subspaces are subsequently scanned by local techniques (conical horn antenna, planar antenna system).

structure	solver	objectives	optimizer	note
time domain beam forming	time domain	time domain	MOSOMA	Pareto front
bow tie antenna	time domain	time domain	PSO	no conflict
high impedance surface	time + eigen-domain	time + eigen-domain	PSO	no conflict
Koch discone	time domain	frequency domain	PSO	no conflict
conical horn antenna	time domain	frequency domain	PSO + local	single objection
planar antenna system	time domain	frequency domain	PSO + local	single objection
semiconductor structure	multi-physics	- - -	parametric	- - -

Tab. 9.1. Overview of compared design problems.

Considering the above given overview, the following conclusions can be formulated:

- Due to the interest in wideband structures, frequency domain solvers are loosing their dominant position which was typical several years ago.

- In case of sophisticated structures (periodic structures, semiconductor ones), several solvers have to be combined (high impedance surfaces), or coupled problems have to be formulated (semiconductor structures).

- Conventional formulation of partial objectives in a cost function is replaced by time domain objectives and multi-domain objectives to eliminate the neces-

sity of transforms. Frequency domain parameters are used to interpret results only.

- Since real-life applications comprise several conflicting objectives, native multi-objective optimizers have to be exploited (MOSOMA, multi-objective PSO, multi-objective genetic algorithms or simulated annealing). Single-objective optimization can be useful in case of simple structures dominantly.

Today's development in numerical design of electromagnetic structures shows the transition from the conventional frequency-domain modeling and design to the time-domain and multi-domain approaches. In this paper, these tendencies have been illustrated by the selected design examples.

Acknowledgements

References

[1.1] BOERINGER, D. W., WERNER, D. H. Bezier representations for the multi-objective optimization of conformal array amplitude weights. *IEEE Transactions on Antennas and Propagation*, 2006, vol. 54, no. 7, p. 1964–1970.

[1.2] FANGLEI SUN; LI, V.O.K.; ZHIFENG DIAO Modified bipartite matching for multi-objective optimization: Application to antenna assignments in MIMO systems. *IEEE Transactions on Wireless Communications*, 2009, vol. 8, no. 3, p. 1349–1355.

[1.3] LU, J., IRELAND, D., LEWIS, A. Multi-objective optimization in high frequency electromagnetics – an effective technique for smart mobile terminal antenna (SMTA) design. *IEEE Transactions on Magnetics*, 2009, vol. 45, no. 3, p. 1072–1075.

[1.4] GOUDOS, S. K., ZAHARIS, Z. D., KAMPITAKI, D. G., REKANOS, I. T., HILAS, C. S. Pareto optimal design of dual-band base station antenna arrays using multi-objective particle swarm optimization with fitness sharing. *IEEE Transactions on Magnetics*, 2009, vol. 45, no. 3, p. 1522–1525.

[1.5] PETKO, J. S., WERNER, D. H. Pareto optimization of thinned planar arrays with elliptical main-beams and low sidelobe levels. *IEEE Transactions on Antennas and Propagation*, 2011, vol. 59, no. 5, p. 1748–1751.

[1.6] CHAMAANI, S., MIRTAHERI, S. A., ABRISHAMIAN, M. S. Improvement of time and frequency domain performance of antipodal Vivaldi antenna using multi-objective particle swarm optimization. *IEEE Transactions on Antennas and Propagation*, 2011, vol. 59, no. 5, p. 1738–1742.

[1.7] JOHNSON, J. M., RAHMAT-SAMII, Y. Genetic algorithms in engineering electromagnetics. *IEEE Antennas and Propagation Magazine*, 1997, vol. 39, no. 4, p. 7–25.

[1.8] ROBINSON, J., RAHMAT-SAMII, Y. Particle swarm optimization in electromagnetics. *IEEE Transactions on Antennas and Propagation*, 2004, vol. 52, no. 2, p. 397–407.

[1.9] KADLEC, P., RAIDA, Z. Comparison of novel multi-objective self-organizing migrating algorithm with conventional methods. In *Proceedings of the 21st International Conference Radioelektronika*. Brno (Czech Republic), p. 97–100, 2011.

[1.10] YUAN, M., SARKAR, T. K., KOLUNDZIJA, B. Solution of large complex problems in computational electromagnetics using higher-order basis in MoM with out-of-core solvers. *IEEE Antennas and Propagation Magazine*, 2006, vol. 48, no. 2, p. 55–62.

[1.11] HODGES, R. E., RAHMAT-SAMII, Y. An iterative current-based hybrid method for complex structures. *IEEE Transactions on Antennas and Propagation*, 1997, vol. 45, no. 2, p. 265 – 276.

[1.12] JIAYUAN FANG, ZHONGHUA WU Generalized perfectly matched layer-an extension of Berenger's perfectly matched layer boundary condition. *IEEE Microwave and Guided Wave Letters*, 1995, vol. 5, no. 12, p. 451–453.

[1.13] KHEBIR, A., KOUKI, A. B., MITTRA, R. Asymptotic boundary conditions for finite element analysis of three-dimensional transmission line discontinuities. *IEEE Transactions on Microwave Theory and Techniques*, 1990, vol. 38, no. 10, p. 1427–1432.

[2.1] FROST, O. L. An algorithm for linearly constrained adaptive array processing. *Proc. of the IEEE*, 1072, vol. 60, no. 8, p. 926 to 935.

[2.2] FENN, A. J., KING, G. A. Experimental investigation of an adaptive feedback algorithm for hot spot reduction in radio-frequency phased-array hyperthermia. *IEEE Transaction on Biomedical Engineering*, 1996, vol. 43, no. 3, p. 273–280.

[2.3] KADLEC, P., ŠTUMPF, M., RAIDA, Z. Adaptive beam forming in time-domain. In *Proceedings of the International Conference on Electromagnetics in Advanced Applications ICEAA 2011*. Torino (Italy), accepted for publication.

[2.4] ŠTUMPF, M., DE HOOP, A. T., LAGER, I. E. Closed-form time domain expressions for the 2D pulsed EM field radiated by an array of slot antennas with finite width. In *Proc. of the Int. Symp. on Electromagnetic Theory*, Berlin (Germany), p. 703–706, 2010.

[2.5] KADLEC, P., RAIDA, Z. A novel multi-objective self-organizing migrating algorithm. *Radioengineering,* 2011, vol. 20, no. 4, p. 804-816.

[3.1] RAO, S. M. *Time Domain Electromagnetics*. London: Academic Press, 1999.

[3.2] LACIK, J., RAIDA, Z. Modeling microwave structure in time domain using Laguerre polynomials. *Radioengineering*, 2006, vol. 15, no. 3, p. 1–9.

[3.3] LACIK, J., LAGER, I. E., RAIDA, Z. Multicriteria optimization of antennas in time domain. *Radioengineering*, 2010, vol. 19, no. 1, p. 105–110.

[3.4] ROBINSON, J., RAMAT-SAMII, Y. Particle swarm optimization in electromagnetics. *IEEE Transactions on Antennas and Propagation*, 2004, vol. 52, no. 2, p. 397–407.

[3.5] RAO, S. M., WILTON, D. R., GLISSON, A. W. Electromagnetic scattering by surfaces of arbitrary shape. *IEEE Transactions on Antennas and Propagation*, 1982, vol. 30, no. 3, p. 409–418.

[4.1] SIEVENPIPER, D., ZHANG, L., BROAS, R. F. J., ALEXOPOULOS, N. G., YABLONOVITCH, E. High-impedance electromagnetic surfaces with a forbidden frequency band. *IEEE Transactions on Microwave Theory and Techniques*, 1999, vol. 47, no. 1, p. 2059–2074.

[4.2] CLAVIJO, S., DIAZ, R. E., MCKINZIE, W. E. Design methodology for Sievenpiper high-impedance surfaces: an artificial magnetic conductor for positive gain electrically small antennas. *IEEE Transactions on Antennas and Propagation*, 2003, vol. 51, no. 10, p. 2678–2690.

[4.3] KOVACS, P., RAIDA, Z. Global evolutionary algorithms in the design of electromagnetic band gap structures with suppressed surface waves propagation. *Radioengineering,* 2010, vol. 19, no. 1, p. 122–128.

[5.1] ELKAMEHOUCHI, H. M., EL-SALAM, M. N. A. Disc-cone antenna design using conducting wires and fractal geometry. In *Proceedings of the Radio Science Conference*, 2008. National Digital Object Identifier: 10.1109/NRSC.2008.4542312, 2008, p. 1–8.

[5.2] BALLESTER, P. J., CARTER, J. N. An effective real-parameter genetic algorithm with parent centric normal crossover for multimodal optimization. In *Proceedings of the Genetic and Evolutionary Computation Conference GECCO'04*. Seattle (USA), 2004, Springer-Verlag, 2004, p. 901–913.

[6.1] BALANIS, C. A. *Antenna Theory: Analysis and Design*. 2nd Edition. New York: John Wiley and Sons, 1997.

[6.2] JORDAN, E. C., BALMAIN, K. G. *Electromagnetic Waves and Radiating Systems*. 2nd Edition. Englewood Cliffs: Prentice Hall, 1968.

[6.3] POCHAZKA, M. *Antennas – Handbook*. 3rd Edition. Prague: BEN Publishing, 2005 (in Czech).

[7.1.] OOI, B.-L., QUIN, S., LEONG, M.-S. Novel design of broad-band stacked patch antenna. *IEEE Transaction on Antennas and Propagation,* 2002, vol. 50, no. 10, p. 1391–1395.

[7.2.] LEVINE, E., MALAMUD, S., SHTRIKMAN, S., TREVES, D. A study of microstrip array antennas with feed network. *IEEE Transaction on Antennas and Propagation*, 1989, vol. 37, no. 4, p. 426–434.

[8.1] FLEMING, P. L. The active medium propagation device. *Proceedings of the IEEE*, 1975, vol. 63, no. 8, p. 1253–1254.

[8.2] LIOUBTCHENKO, D. V., TRETYAKOV, S., DUDOROV, S. *Millimeter-Wave Waveguides*, Boston: Kluwer Academic Publishers, 2003.

[8.3] POKORNÝ, M. *Modeling of Microwave Semiconductor Structures*, Doctoral thesis, Brno: Brno University of Technology, 2011.

[8.4] REES, H. Hot Electron effect at microwave frequencies in GaAs, *Solid State Communications*, 1969, vol. 7, p. 267–269.

[8.5] SHUR, M. *GaAs Devices and Circuits*. London - New York: Springer, 1987.

[8.6] SZE, S. M. *Physics of Semiconductor Devices*. 3rd edition. Wiley-Interscience, 2007.